Specular and diffuse scattering from random asperities of any profile using the rigorous method for x-rays and neutrons

Leonid I. Goray*[a,b]
[a]St. Petersburg Physics and Technology Center for Research and Education, RAS, Khlopina 8/3, St. Petersburg 195220, Russia
[b]Institute for Analytical Instrumentation, RAS, 26 Rizhsky Pr., St. Petersburg 190103, Russia

ABSTRACT

The present work deals with a comprehensive numerical analysis of x-ray grazing-incidence scattering from single- and double-boundary, finite-conducting rough surfaces with asperities of different statistics, performed with the use of a mid-end workstation in a reasonable computation time. Multiple and multi-wave diffraction, refraction, absorption, and resonances influence significantly x-ray and neutron scattering. These are pure dynamic effects, which require application of a rigorous theory to correctly describe the power change in the specular order and to describe non-specular distribution. Despite the impressive progress attained in developing a rigorous theory with account for random roughness, the author is aware only of approximate and asymptotic approaches in the case of neutron and x-ray scattering even by 1D surfaces, such as the Born approximation, the distorted-wave Born approximation, parabolic equation methods, etc. The PCGrate®-SX v.6.3 software developed on the basis of a modified boundary integral equation method and the Separating solver allows one to operate with exact models, e.g., those involving Maxwell's equations and rigorous boundary conditions, and appropriate radiation conditions. In order to compute the scattering properties of a rough surface using the forward electromagnetic solver, Monte Carlo simulation is employed to average the deterministic scattered power due to individual surfaces over an ensemble of realizations. The difference between approximate and rigorous approaches can be clearly seen in cases where grazing incidence occurs at close to or larger than the critical angle. This difference may give rise to wrong estimates of rms roughness and correlation length if they are determined by comparing experimental data with calculations. Besides, the rigorous approach permits taking into account any known roughness statistics, including quasi-periodicity of quantum dot ensembles.

Keywords: x-ray and neutron scattering, grazing-incidence x-ray reflectometry, random roughness, quantum dots, boundary integral equations, specular and diffuse reflectance, numerical scattering analysis

1. INTRODUCTION

Multi-wave and multiple diffraction, refraction and absorption, resonances and wave deformation govern to a considerable extent scattering from nanoroughness of continuous media and thin films in the x-ray and extreme ultraviolet (EUV) ranges. Account of these pure dynamic effects, which requires application of rigorous electromagnetic theory, permits one to calculate the intensity of the specular component and describe adequately the intensity distribution of the diffuse component which may have resonance peaks. Despite the impressive progress reached recently in development of exact numerical methods of investigation of wave diffraction from boundary roughness[1-3], the present author is aware only of asymptotic and approximate approaches to the analysis of x-ray and neutron scattering, such as the Born approximation (BA), distorted-wave Born approximation (DWBA), method of parabolic wave equation (PWE), and a few others[4, 5].

The rigorous modified method of boundary integral equations[6-9] (MIM), employed widely in analyzing the efficiency of bulk and multilayered diffraction gratings, including those with real border profiles, has been recently extended to cover non-periodic and quasi-periodic structures with border roughness of any type[10]. The method is very accurate and fairly fast convergent in the range of large ratios of period d and boundary depth h to wavelength λ[11], an impressive achievement for any numerical approach[12-18], particularly for structures with randomized borders. The program PCGrate-

*lig@pcgrate.com; phone 7 812 909-7133; fax 7 812 251-7038; pcgrate.com

Modeling Aspects in Optical Metrology II, edited by Harald Bosse, Bernd Bodermann, Richard M. Silver,
Proc. of SPIE Vol. 7390, 73900V · © 2009 SPIE · CCC code: 0277-786X/09/$18 · doi: 10.1117/12.827444

SX® v.6.3[19], which has been developed in the frame of rigorous theory (i.e., with the use of Maxwell's equations, rigorous boundary and radiation conditions), permits application of optical methods to analysis of specular and non-specular x-ray scattering from multilayer rough mirrors in real space. For rigorous account of roughness, PCGrate-SX® v.6.3 makes use of a model, in which a randomized surface is identified with a grating with a large d containing a large number of random asperities. Thus, the program analyzes complex structures ,which may be considered as gratings from the pure mathematical standpoint while representing in actual fact a rough surface if d is chosen much larger than the correlation length (width) ζ of the asperities. Furthermore, in cases where ζ is comparable with λ, and the number of orders is large, the continuous angular distribution of diffuse power reflected from a randomized boundary can be described by a discrete angular distribution of grating efficiency.

To study the scattering intensity with the use of a forward electromagnetic code and Monte Carlo simulation, one should first of all generate statistical realizations of the boundary profiles of the structure under investigation, then calculate the scattering intensity for each realization and, finally, average the intensities over all the realizations. The present author used a spectral method[20] to generate plane surfaces with a Gaussian height distribution and a Gaussian correlation function. To allow randomization of grating boundaries, this method was extended to cover the case of non-flat interfaces prescribed by arbitrary polygons[19]. In particular, non-plane boundaries are characteristic of self-assembled low-dimensional quantum structures defined by other asperity statistics[21]. The present paper addresses rigorous simulation of grazing-incidence x-ray reflectometry (GIXRR) as applied to continuous and single-layer, finite-conducting 1D surfaces with random and quasi-regular roughness in the case of ray incidence in the plane perpendicular to the relief (classical 2D diffraction). Data obtained by approximate methods and the rigorous approach are found to be noticeably different, however, in the cases of near-normal incidence, arbitrary incident beam orientation, perfect conductivity of the lower boundary, multilayer mirrors and randomized diffraction gratings as well, a problem to be considered elsewhere.

2. APPROXIMATION METHODS

Scattering from rough surfaces modifies significantly the power distribution between the reflected and transmitted specular fields and generates additional losses due to absorption within the media. The existing theoretical frameworks exploit the fact that interaction between x-rays and matter is typically weak ("small roughness approximation") or, alternatively, the surface is very rough whose typical length scales are much greater than the wavelength. In the first case, one treats the specular and non-specular scattering from interfacial roughness using first- or, at most, second-order perturbation theory. Hence the theory is limited to the case where the non-specular scattered power is small compared to the incident power. In the second case of the geometrical optics approximation (scalar theory), one launches a large number of parallel incident rays on the surface, hence the polarization and resonance effects in this model are non-accountable. For the strictly grazing scattering the PWE method can be explored for such directed waves and arbitrary roughnesses.

Within the context of the geometrical optics theory (or the high-frequency Kirchhoff integral approximation), each ray undergoes a series of reflections off the surface until it finally escapes[5]. A fundamental constraint on the application of this approach to bulk and multilayer x-ray structures, as well as to those with one dielectric coating, is imposed by the large slopes and oblique angle of incidence, which should not be very close to grazing[8]. The critical value of the angle depends, however, on the actual surface parameters and the light wavelength and polarization. The limitation on the angle of incidence is connected with the difference in scattering between the finitely and perfectly conducting bulk rough mirrors operating in the x-ray range under grazing incidence, particularly in the case of the TM polarization.

Turning now to perturbation theory, two different formulations are basically used for x-rays and neutrons, each valid in its specific regime. The BA is based on iterative solution of an integral equation and was first applied to homogeneous rough surfaces in the context of x-ray and neutron scattering[4]. The BA refers to a family of methods in which the unknown field satisfies a volume integral equation of the second kind, with a 'potential' term and the Green's function in the integrand. The solution can then formally be expressed as an iteration series (the so-called Born or Neumann series) with the potential used as a small parameter[8,22]. The Born approximation usually corresponds to the first iteration. The small parameter of this expansion is typically the electric permittivity contrast, which is very small for x-rays and

neutrons. The main weakness of the BA is that it does not take properly into account refraction by the surface and, therefore, fails as one approaches the so-called critical angle, at which total external reflection occurs. The BA can be improved considerably in this respect by choosing a more appropriate reference problem, namely, a flat surface between two media. In this case, the free-space Green function is replaced by a half-space Green function, that depends explicitly on the Fresnel reflection coefficient at the plane interface. This is the so-called DWBA, a method which draws inspiration from methods, as the BA, of quantum mechanics and was developed in the eighties of the last century for x-ray scattering from rough surfaces[4]. The expression derived from the second-order DWBA connects smoothly the expressions derived from the BA and first-order DWBA approximations[23].

If the fields near a rough surface travel predominantly in one direction, a parabolic approximation to Maxwell's equation about the direction of propagation can be employed as a basis for a numerical method[1]. The PWE approximation neglects large-angle and multiple scattered waves that turn back on themselves, and reduces computational cost by employing a marching method in the direction of wave propagation.

The Debye-Waller (DW) asymptotic, which can be derived from the BA, is commonly used in this region where grazing angle of incidence on the plane must be large and far from the critical angle[10,24]. The Nevot-Croce (NC) model, which can be derived from the first-order DWBA, is used mostly at grazing incidence near or below the critical angle. Both descriptions of the reduction of specular reflectance are valid, strictly speaking, in the case of small roughness heights (rms roughness σ) and very big (DW) or very small (NC) correlation lengths. It was shown[25] and corroborated by our calculations[26] that the correlation function, which determines the properties of scattering from shallow nanorough surfaces, becomes no longer adequate for description of the speckle pattern after the mean height of irregularities h has exceeded one-tenth of the wavelength. The use of the above or even more sophisticated approximations in the intermediate incident angle range, for high conducting surfaces, and especially in the TM polarization also appears very questionable.

3. SEPARATING SOLVER

The PCGrate 6.3 Separating solver of the MIM is based on the single-boundary integral-equation Scattering solver[19] and the Scattering-matrix approach to multilayer diffraction [14,27,28]. By definition, it requires that a homogeneous medium separate two adjacent corrugated regions by fictitious planes[10]. The distance between such planes may be arbitrary, including very nearly zero separation. The Separating solver is primarily intended for intensity calculations for any uncoated, including rough, grating and mirror, specific types of coated gratings, and photonic crystals. It is indispensable for x-ray and EUV gratings and mirrors covered with one or many plane or rather thick conformal coatings and, especially, for grazing incidence structures. In this Section the Separating solver is described for the general case of conical diffraction and arbitrary polarization.

3.1 Field representations in a homogeneous plane layer between corrugated regions

Consider scattering by a grating structure of elliptically-polarized light with the wave vector $\mathbf{k}$, vectors of the electrical field $\mathbf{E}$ and magnetic field $\mathbf{H}$, and the phase difference angle $\psi = \psi_2 - \psi_1$ between the polarization components TM (S) and TE (P). Due to geometric invariance of the physical problem with respect to the z coordinate and time t, we come to

$$\mathbf{E}(x, y, z, t) = \mathbf{E}(x, y)\exp\{i(k_z z - i\omega t)\} = \mathbf{E_0}(x, y)\exp(-i\psi_1)\exp\{i(k_z z - i\omega t)\}; \quad (1a)$$
$$\mathbf{H}(x, y, z, t) = \mathbf{H}(x, y)\exp\{i(k_z z - i\omega t)\} = \mathbf{H_0}(x, y)\exp(-i\psi_2)\exp\{i(k_z z - i\omega t)\}, \quad (1b)$$

where the z-component $k_{z,l} = \gamma_l$ of the wave vector in layer l can be described by the relations

$$\mathbf{k_{m,l}} = \alpha_{m,l}\mathbf{x} - \beta_{m,l}\mathbf{y} + \gamma_l\mathbf{z};\ \alpha_{m,l} = 2\pi(\sqrt{\mu_l}\sqrt{\varepsilon_l}\sin(\theta_l)\cos(\varphi_l)/\lambda + m/d);$$
$$\gamma_l = 2\pi\sqrt{\mu_l}\sqrt{\varepsilon_l}\sin(\varphi_l)/\lambda;$$
$$\beta_{m,l} = [(2\pi\sqrt{\mu_l}\sqrt{\varepsilon_l}/\lambda)^2 - (\alpha^2_{m,l} + \gamma^2_l)]^{0.5} \text{ or}$$
$$\beta_{m,l} = i[\alpha^2_{m,l} + \gamma^2_l - (2\pi\sqrt{\mu_l}\sqrt{\varepsilon_l}/\lambda)^2]^{0.5}, \quad (2)$$

where λ is the wavelength in vacuum. Because of the operator £ transforming the incident into total (and diffraction) field being linear, the z-dependence of the incident and diffracted field is the same and, in the particular case of the conical problem, can be dropped. Denote the m-th order wave vector in the layer l with the cut-off z-component by $\kappa_{m,l}$:

$$\kappa^2_{m,l} = |\mathbf{k}_{m,l}|^2 - \gamma^2_l. \tag{3}$$

Substituting (1) into Maxwell's equations and recalling the boundary conditions, we come to the Helmholtz equations for the z-components E_z and H_z in each homogeneous layer l for piecewise constant values of $\kappa_{0,l}$

$$\Delta E_z - \kappa^2_{0,l} E_z = 0; \tag{4a}$$
$$\Delta H_z - \kappa^2_{0,l} H_z = 0. \tag{4b}$$

The explicit form of boundary conditions of the transmission type, together with the analytic properties of integral operators, as well as other notations can be found in[29]. Thus, to solve the conical diffraction problem, one needs to find only the z-components of the electric and magnetic field. Knowing them, one can readily derive the other field components.

3.2 Derivation of the complex field amplitudes in the layers using Rayleigh expansions

For the fields in the upper and lower half-infinite media, as well as for homogeneous layers that can be separated between two adjacent boundaries Γ_{l-1} and Γ_l by planes, the Rayleigh expansion is valid. For the fields in the coordinate system attached to the lower boundary Γ_l we have

$$E_{z,l}(x, y) = \sum_{m=-\infty}^{\infty} C^{P}_{m,l} \exp\{i(\alpha_{m,l}x - \beta_{m,l}y_l)\} + \sum_{m=-\infty}^{\infty} D^{P}_{m,l} \exp\{i(\alpha_{m,l}x + \beta_{m,l}y_l)\}; \tag{5a}$$
$$H_{z,l}(x, y) = \sum_{m=-\infty}^{\infty} C^{S}_{m,l} \exp\{i(\alpha_{m,l}x - \beta_{m,l}y_l)\} + \sum_{m=-\infty}^{\infty} D^{S}_{m,l} \exp\{i(\alpha_{m,l}x + \beta_{m,l}y_l)\}. \tag{5b}$$

For those in the coordinate system attached to the upper boundary Γ_{l-1} ($l = 1$ denotes the superstrate boundary, and $l = L$ denotes the substrate boundary) we have

$$E_{z,l}(x, y) = \sum_{m=-\infty}^{\infty} A^{P}_{m,l-1} \exp\{i(\alpha_{m,l}x - \beta_{m,l}y_{l-1})\} + \sum_{m=-\infty}^{\infty} B^{P}_{m,l-1} \exp\{i(\alpha_{m,l}x + \beta_{m,l}y_{l-1})\}; \tag{6a}$$
$$H_{z,l}(x, y) = \sum_{m=-\infty}^{\infty} A^{S}_{m,l-1} \exp\{i(\alpha_{m,l}x - \beta_{m,l}y_{l-1})\} + \sum_{m=-\infty}^{\infty} B^{S}_{m,l-1} \exp\{i(\alpha_{m,l}x + \beta_{m,l}y_{l-1})\}. \tag{6b}$$

We shall subsequently write the same expressions for the coefficients of the electrical and magnetic field component harmonics, bearing in mind they are actually two different sets of coefficients with indices P(TE) and S(TM). The Rayleigh coefficients $A_{m,l}$, $B_{m,l}$, $C_{m,l-1}$, $D_{m,l-1}$ are coupled through the relations

$$C_{m,l-1} = A_{m,l} \exp\{i(-\beta_{m,l}e_l)\}; \tag{7a}$$
$$D_{m,l-1} = B_{m,l} \exp\{i(+\beta_{m,l}e_l)\}, \tag{7b}$$

where e_l denotes vertical shift between the boundaries Γ_{l-1} and Γ_l:

$$e_l = y_{l-1} - y_l. \tag{8}$$

3.3 Matrix relations for reflection and transmission amplitude factors

We denote

$$C_{l-1} = U_l A_l; \tag{9a}$$
$$D_{l-1} = U'_l B_l, \tag{9b}$$

where A_l, B_l, C_{l-1}, D_{l-1} and U_l and U'_l are the corresponding column and diagonal matrices, respectively. Each boundary is characterized by two reflection and two transmission matrices, which are related through

$$B_l = t'_l D_l + r_l A_l; \quad (10a)$$
$$C_l = r'_l D_l + t_l A_l. \quad (10b)$$

Consider a stack of $L - l$ lower interfaces. For the lowest $l = L$ layer $D_L = 0$, because our physical problem does not include waves coming from the substrate. Then, for the upper layer l

$$B_l = R_l A_l; \quad (11a)$$
$$C_L = T_l A_l. \quad (11b)$$

To solve the problem, we have to find the reflection and transmission matrices R_1 and T_1 from known matrices R_L and T_L:

$$R_L = r_L, \quad (12a)$$
$$T_L = t_L. \quad (12b)$$

We can derive the relations coupling R_{l-1} and T_{l-1} with R_l and T_l by invoking (9) and (10) in conjunction with (11) and (12):

$$R_{l-1} = r_{l-1} + (t'_{l-1} U'_l R_l)(U_l - r'_{l-1} U'_l R_l)^{-1} t_{l-1}; \quad (13a)$$
$$T_{l-1} = T_l (U_l - r'_{l-1} U'_l R_l)^{-1} t_{l-1}. \quad (13b)$$

Expressions (13a) and (13b) allow us to find R_1 and T_1 by a recursive procedure beginning with the lower medium labeled by L[14,27,28]. To do this, we have to know, in a general case, eight matrices of scattering amplitudes (two full scattering amplitude matrices for the S and P polarization components) and perform two matrix inversions in each iteration step.

3.4 Efficiencies and polarization angles

For the incident wave amplitude we use unit normalization of the type

$$(\beta_{0,0}/\kappa^2_{0,0})(\varepsilon_0 |E_{z,inc}|^2 + \mu_0 |H_{z,inc}|^2) = 1. \quad (14)$$

Then for the diffraction efficiencies we can write

$$\xi_{m,0} = (\beta_{m,0}/\kappa^2_{0,0})(\varepsilon_0 |B_1^P|^2 + \mu_0 |B_1^S|^2); \quad (15a)$$
$$\xi_{m,L} = (\beta_{m,L}/\kappa^2_{0,L})(\varepsilon_L |C_L^P|^2 + \mu_0 |C_L^S|^2). \quad (15b)$$

The generalized energy balance leads us to

$$\sum_m \xi_{m,0} + \sum_{m'} \xi_{m',L} + \sum_{l=1}^{l=L-1} \varsigma_l = 1, \quad (16)$$

where ς_l is the absorption in layer l that can be treated separately[30].

By definition, the polarization angles of the incident[31] and m-th diffracted waves in the l layer can be found from the s (P) and p (S) components of the electric field $E^P_{m,l}$ and $E^S_{m,l}$, respectively:

$$\delta_{m,l} = \mathrm{arctg}(|E^P_{m,l}| / |E^S_{m,l}|); \quad (17a)$$
$$\psi_{m,l} = -\arg(E^P_{m,l} / E^S_{m,l}), \quad (17b)$$

where $0 \le \delta_{m,l} \le \pi/2$, $\pi < \psi_{m,l} \le \pi$,

$$E^P_{m,l} = (\mathbf{E}_{m,l}, \mathbf{s}_{m,l}); \quad (18a)$$
$$E^S_{m,l} = (\mathbf{E}_{m,l}, \mathbf{p}_{m,l}), \quad (18b)$$

and one can associate two unit vectors $\mathbf{s}_{m,l}$ and $\mathbf{p}_{m,l}$, such that

$$\mathbf{s}_{m,l} = \mathbf{k}_{m,l} \times (0, 1, 0) / |\mathbf{k}_{m,l} \times (0, 1, 0)|; \quad (19a)$$
$$\mathbf{p}_{m,l} = \mathbf{s}_{m,l} \times \mathbf{k}_{m,l} / |\mathbf{k}_{m,l}|. \quad (19b)$$

It can also be shown that

$$E^{P}_{m,0}/E^{S}_{m,0} = [\mu_0/\varepsilon_0]^{0.5}(\alpha_{m,0}\varepsilon_0 k_0 B_1^{P} + \beta_{m,0}\gamma_0 B_1^{S})/(\alpha_{m,0}\mu_0 k_0 B_1^{S} - \beta_{m,0}\gamma_0 B_1^{P}); \quad (20a)$$
$$E^{P}_{m,L}/E^{S}_{m,L} = [\mu_L/\varepsilon_L]^{0.5}(\alpha_{m,L}\varepsilon_L k_0 C_L^{P} + \beta_{m,L}\gamma_L C_L^{S})/(\alpha_{m,L}\mu_L k_0 C_L^{S} - \beta_{m,L}\gamma_L C_L^{P}). \quad (20b)$$

where $k_0 = (2\pi/\lambda)$.

In the case of pure polarization and in-plane diffraction, the number of scattering matrices for all boundaries reduces by a factor two.

4. EXAMPLES OF CALCULATIONS

In this Section, we are going to address the results of numerical study of specular grazing-incidence reflection of hard and soft x-rays from gold mirrors with different roughness parameters, as well as illustrate the calculation of specular and diffuse grazing-incidence hard x-ray reflectivities from quasi-regular Ge(Si)/Si QDs. Readers interested in investigation of specular and diffuse x-ray scattering from multiple ensembles of In(Ga)As/GaAs QDs performed in the frame of the MIM are referred to[21].

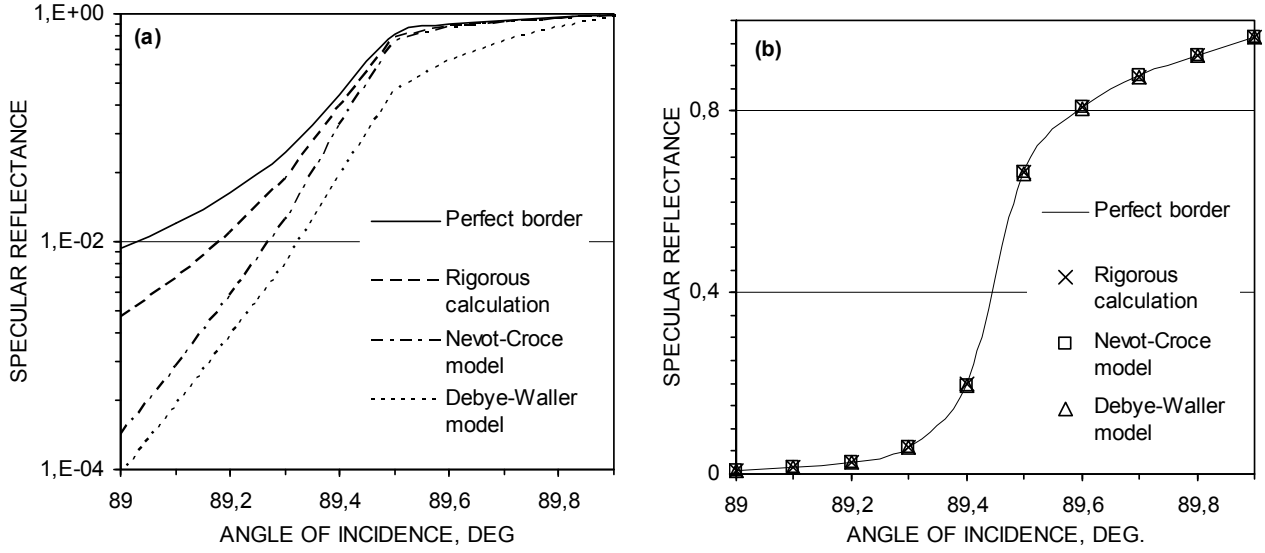

Fig. 1. TE reflectance models of Au mirrors ($\lambda = 0.154$ nm) plotted vs. angle of incidence for different σ and ζ. (a) $\sigma = 0$ and $\zeta = \infty$ (solid line – perfect surface); $\sigma = 1.5$ nm and $\zeta = 5$ nm (long-dashed line – rigorous average model for 15 random borders); $\sigma = 1.5$ nm and $\zeta = 0$ (long-short-dashed line – NC model); $\sigma = 1.5$ nm and $\zeta = \infty$ (short-dashed line – DW model).
(b) $\sigma = 0$ and $\zeta = \infty$ (solid line – perfect surface); $\sigma = 0.15$ nm and $\zeta = 5$ nm (crosses – rigorous average model for 15 random borders); $\sigma = 0.15$ nm and $\zeta = 0$ (squares – NC model); $\sigma = 0.15$ nm and $\zeta = \infty$ (triangles – DW model).

4.1 Specular reflectivity of Au mirrors

A bulk model of a typical gold x-ray mirror for use at grazing incidence near the angle of total external reflection was chosen as a sample. The difference between the asymptotic and rigorous approaches can be clearly seen in the figures

which plot the calculated specular TE reflectances (TM reflectance data are close in magnitude) of Au surfaces vs. the angle of incidence for different values of σ, ζ, and λ. For the DW model, ζ = ∞, for the NC model, ζ = 0, and for the rigorous model, chosen ζ are close to the asymptotic values or have intermediate values. The refractive indices of Au were taken from[32].

A comparison between the approximate and rigorous models for Cu $K\alpha_1$ radiation (λ = 0.154 nm), ζ = 5 and different σ is shown in Fig. 1. For σ = 1.5 nm in Fig. 1 (a), the difference is about an order of magnitude in the low reflectance range, and about a few times in the intermediate range. Close to the critical angle, this excess amounts to ~10% compared with the figure derived from the NC asymptotics. Such pronounced differences may bring about an overestimation of σ if it is deduced from a comparison of experimental data with calculations[24]. For σ = 0.15 nm (Fig. 1(b)), the results obtained for all the models differ only by a few % within the angular range studied. Significantly, only 10-15 random asperities within *d* and about as many statistical realizations turned out to be sufficient for the average values of the reflectance in the examples of Fig. 1 to converge. The number of collocation points at the border required to reach convergence and the desired accuracy (~1.E–5) as estimated from the energy balance was found to be 2000[11]. Note that in the deep roughness case, the convergence speed-up techniques were used. The time taken up by one rigorous computation on a workstation with two Quad-Core Intel® Xeon® 2.66 GHz processors, 8 MB L2 Cache, 1333 MHz Bus Clock and 16 GB RAM, is ~16 min when operating on Windows Vista® Ultimate 64-bit and employing eightfold paralleling.

A typical border profile used for modeling of such rough mirrors, which have a period of 50 nm, σ = 1.5 nm, and ~10 asperities per period is demonstrated in Fig. 2 (a). To reach the required average statistical depth with due allowance for the fine structure of the roughness in the above example, one has to use at least 10 sample points per asperity. The heights of randomized borders range from 3 nm to 15 nm. Thus, the *h*/λ ratio may reach 100, a figure very large for any numerical method.

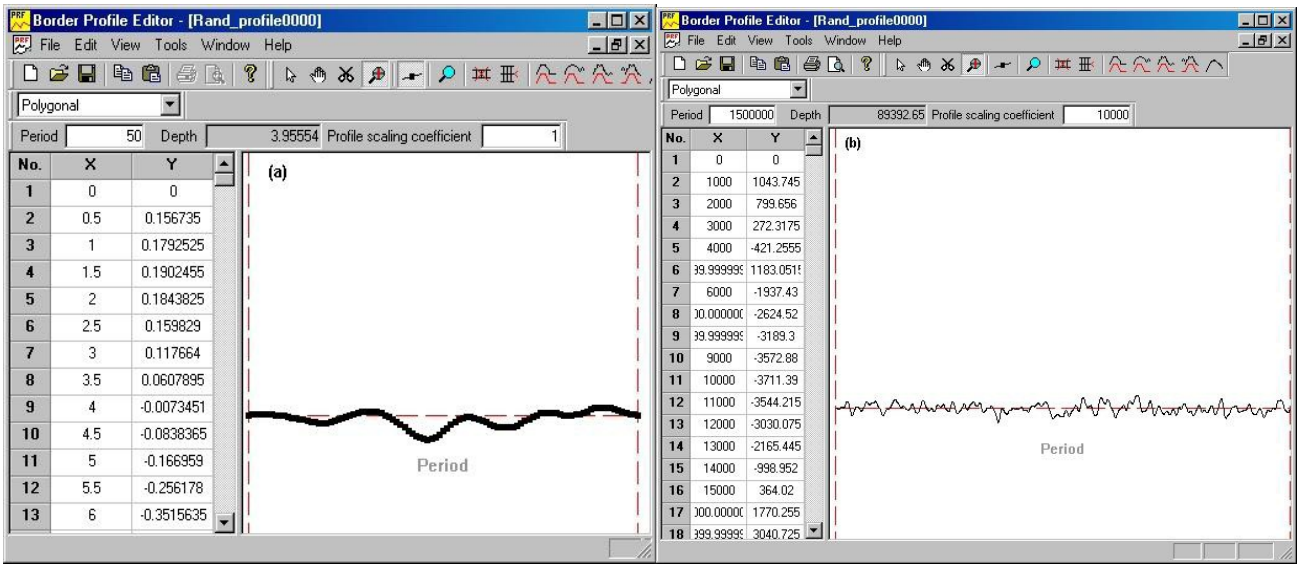

Fig. 2. A border profile sample used in rigorous models of Au x-ray mirrors: (a) *d* = 50 nm, σ = 1.5 nm ζ = 5 nm; (b) *d* = 1500 μm, σ = 1.5 nm ζ = 10 μm, and scales differ by a factor 10^4.

Figure 3 compares the approximate and rigorous models for λ = 0.154 nm, σ = 1.5 nm and different ζ. The reflection coefficients calculated rigorously in the low-intensity domain (Fig. 3 (a)) for ζ = 10 μm are approximately twice those obtained with the DW asymptotics. For ζ = 0.1 μm, the excess is already about fourfold. By contrast, close to the critical angle (Fig. 3 (b)) the rigorous data obtained for ζ = 0.1 μm lie ~20% below the values calculated for this region with the NC factor. For ζ = 10 μm, in the region of high intensities, the differences are still larger, to reach finally a few hundred %. Such pronounced differences may give rise not only to overestimation of σ, but to a wrong assessment of ζ as well, if they are deduced from a comparison of experimental with calculated data[10]. The behavior of the scattering intensity on ζ which is

illustrated graphically in Fig. 3 matches qualitatively with the results obtained in the frame of the second-order DWBA, while differing clearly in quantitative estimates, particularly for values of ζ for which second-order DWBA does not work[23].

A typical border profile used for modeling of such rough mirrors, which have d = 1500 μm, σ = 1.5 nm, and ζ = 10 μm, is demonstrated in Fig. 2 (b) (vertical scales differ by a factor 10^4). To account for the fine structure of irregularities in the above example, one has to use ~100 asperities per d, several sample points per asperity, average over 9-25 random boundaries and assume 400-3200 collocation points. For ζ = 10 μm and d = 1500 μm, λ / d ≈ 1.E–7, a value too small to be dealt with in any known rigorous numerical approach. For the Separating solver of the MIM, however, this formidable scattering problem is found to be convergent and yields quite accurate results (Energy balance error ~1.E–6) for only 400 collocation points used and no speed-up techniques invoked[11]. The time taken up by one computation on the above mentioned workstation is ~40 sec.

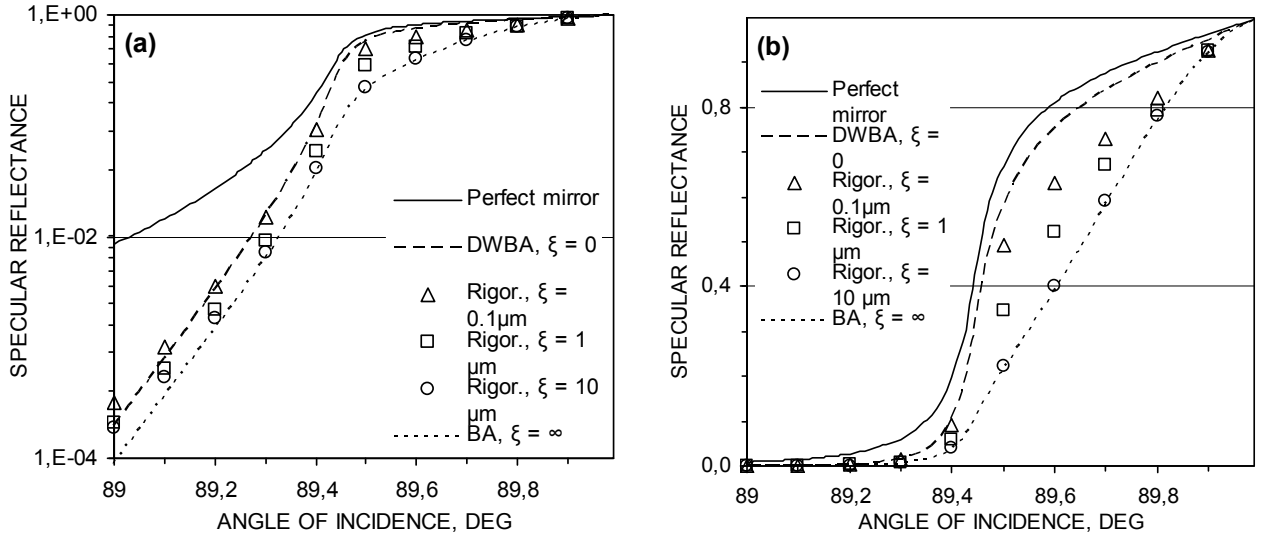

Fig. 3. Specular TE reflectance of Au surfaces calculated for rms roughness σ = 1.5 nm and different correlation lengths ζ for λ = 0.154 nm and plotted vs. angle of incidence on (a) logarithmic and (b) linear scales.

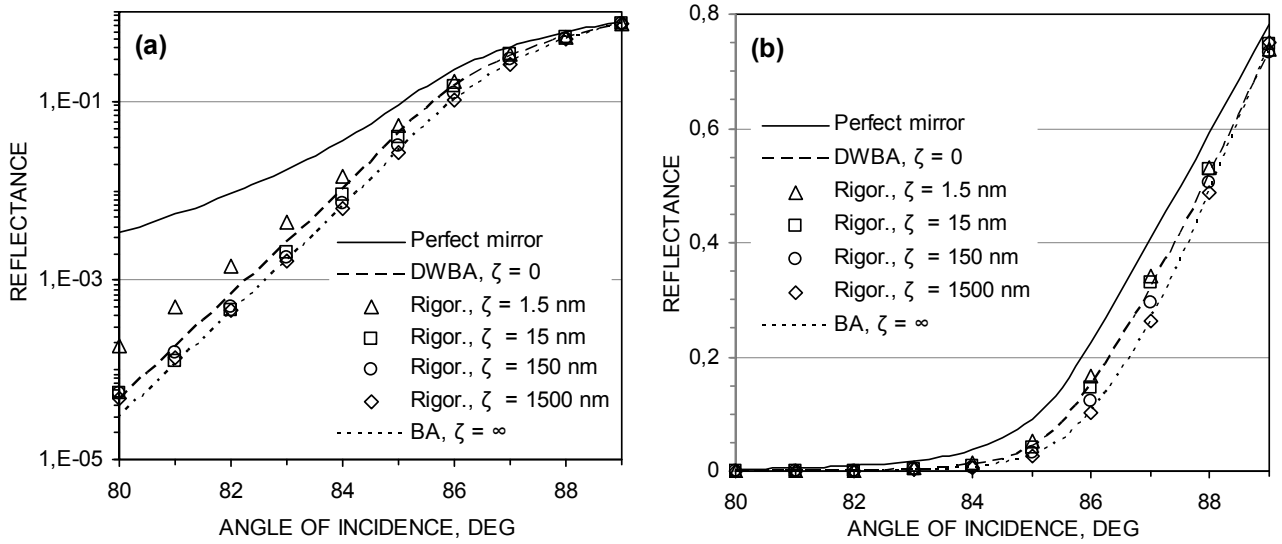

Fig. 4. Specular TE reflectance of Au surfaces calculated for rms roughness σ = 1.5 nm and different correlation lengths ζ for λ = 1.5 nm and plotted vs. angle of incidence on (a) logarithmic and (b) linear scales.

Figure 4 plots graphs similar to those presented earlier but obtained for λ = 1.5 nm, σ = 1.5 nм and different ζ. For the minimum ζ = 1.5 nm, the rigorous results exceed by a few times those derived from the DW asymptotics for large grazing angles, and are ~10% larger than the ones extracted from the NC asymptotics close to the critical angle. For ζ = 15 nm, the differences are smaller, and as the correlation length continues to grow, rigorous calculations yield results which approach throughout the angular range covered the values derived from the DW asymptotics, in full agreement with[23]. In the examples with λ = 1.5 nm, one has to take into account ~50 asperities per *d*, average over 9-25 random borders and use 200-2400 collocation points. None of the known convergence speed-up techniques was applied in these cases.

4.2 Specular and diffuse reflectivity of Ge/Si quantum dots

A recent GIXRR study has analyzed x-ray scattering from samples with multiple QD ensembles grown in the In(Ga)As/GaAs system[21]. In the model, QDs are ordered on the average and have the randomized pyramid (triangle in the cross section) shape[10]. The position of the experimentally observed diffuse-scattering intensity peaks was found to be totally determined by the slope angle α of the QD faces (the so-called diffraction grating blaze condition)[21], which had been theoretically predicted earlier[10]. A comparison with the results of numerical modeling of scattering based on the MIM suggests that a straightforward geometric condition $2\alpha = \theta_{inc} \pm \theta_{diff}$ permits one to accurately derive α from the position of the intensity peak whose shape depends on many parameters. In this Section, we are going to illustrate calculation of the coefficients of specular and diffuse x-ray reflection from quasi-regular Ge QDs grown on a Si substrate. The refractive indices of Ge and Si were taken from[32].

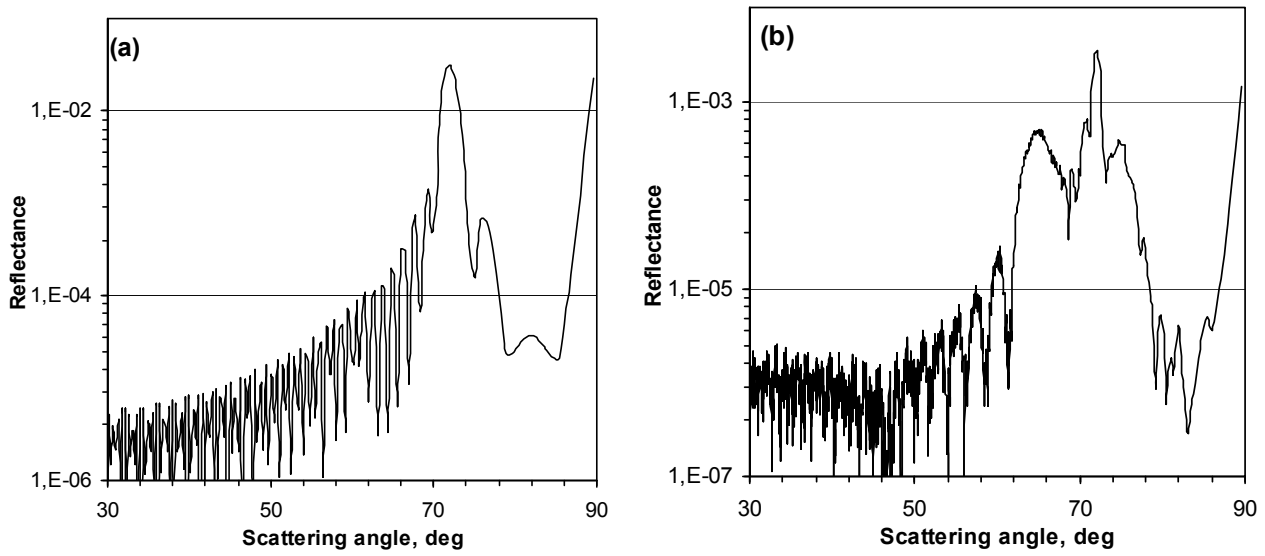

Fig. 5. Specular and diffuse reflectivity of Ge/Si QD structures calculated for λ = 0.154-nm and 89.6º incidence and plotted vs. angle of scattering for: (a) model of the pyramid asperity type with one preferable face slope angle; (b) model of the dome asperity type with several preferable face slope angles.

Typical theoretical curves of specular and diffuse scattering intensities obtained with the use of GIXRR for Ge/Si QD structures are shown graphically in Figs. 5 (a) and 5 (b). The position and shape of the main peaks in both graphs correlate well with the measurements[33]; to compare their amplitudes, however, one should reduce the three-dimensional scattering problem to the two-dimensional one[21]. A few sets of generated border parameters are enough to compute exact efficiencies of such a model. The error of the calculations estimated from the energy balance was ~1.E–6 for 400-1600 collocation points at each boundary of the modeled structures. The time taken up by calculations of a scattering intensity curve with one statistical set of parameters on the above mentioned workstation is ~2 min. Note that the convergence speed-up techniques were used in this deep irregularity case.

5. SUMMARY

The most essential results of the present study can be summed up as follows.

Calculations based on rigorous electromagnetic theory were performed using the MIM, which turned out to provide high accuracy and fast convergence for very large ratios of the characteristic period and height to wavelength. The presented Separating solver of the MIM gives exact results and works fast in the x-ray range at grazing incidence, the most difficult case for any rigorous numerical code.

Diffraction problems with 1D bulk and single-layer structures with arbitrary border profiles, including edges and random asperities, are treated with the PCgrate-SX v.6.3 Separating solver. Rigorous accounting of asperities having Gaussian and non-Gaussian surface statistics has been applied to diverse problems and parameters: (1) x-ray specular reflectance of Au mirrors for different rms roughnesses, correlation lengths, and wavelengths; (2) x-ray diffuse and specular reflectances of single-layer QDs.

The accurate results obtained by the rigorous method for the intensity of x-ray scattering by randomly rough mirrors and quasi-periodical QDs may differ substantially from those derived using known asymptotics and approximate approaches. These differences may give rise, for instance, to wrong estimates of rms roughness and correlation length (slope angles) if they are determined by comparing experimental data with calculations. Besides, the rigorous approach permits taking into account any known roughness statistics.

The proposed approach to numerical treatment of x-ray diffraction from low-dimensional structures like QD ensembles permits one to determine accurately the specular and the diffuse reflectance components. Both theoretical and experimental studies have revealed that the angular diffuse spectrum of scattering from QDs contains resonances corresponding to specular reflection from QD faces. The positions of the resonances should yield the angular slopes of QDs derived from a simple geometric relation with a high accuracy were corroborated by exact calculations. Thus, the traditional use of XRR in determination of layer parameters and of boundary imperfections has been extended to provide a method taking into account the geometry of QDs epitaxially grown in different systems.

ACKNOWLEDGEMENTS

The author feels indebted to Sergey Sadov (New Foundland Memorial University, Canada) for the information provided and fruitful collaboration. Helpful discussions and testing with Bernd Kleemann (Carl Zeiss AG, Germany), Andreas Rathsfeld (WIAS, Germany), and Gunther Schmidt (WIAS, Germany) are greatly appreciated.

Partial support of the Russian Foundation for Basic Research is gratefully acknowledged.

REFERENCES

[1] Warnick, K. F. and Chew, W. C., "Numerical simulation methods for rough surface scattering," Waves Random Media 11(1), R1-R30 (2001).
[2] Saillard, M. and Sentenac, A., "Rigorous solutions for electromagnetic scattering from rough surfaces," Waves Random Media 11(3), R103-R137 (2001).
[3] Déchamps, N., Beaucoudrey, N., Bourlier, C. and Toutain S., "Fast numerical method for electromagnetic scattering by rough layered interfaces: Propagation-inside-layer expansion method," J. Opt. Soc. Am. A 23(2), 359-369 (2006).
[4] Elfouhaily, T. M. and Guérin C.-A., "A critical survey of approximate scattering wave theories from random rough surfaces," Waves Random Media 14(1), R1-R40 (2004).
[5] Babich, M. V. and Buldyrev, V. S., [Asymptotic Methods in Short-Wavelength Diffraction Theory], Alpha Science Series on Wave Phenomena, Oxford (2007).

[6] Goray, L. I., Seely, J. F. and Sadov, S. Yu., "Spectral separation of the efficiencies of the inside and outside orders of soft-x-ray–extreme ultraviolet gratings at near normal incidence," J. Appl. Phys. 100, 094901-1-13 (2006).
[7] Goray, L. I., Kuznetsov, I. G., Sadov, S. Yu. and Content, D. A., "Multilayer resonant subwavelength gratings: effects of waveguide modes and real groove profiles," J. Opt. Soc. Am. A 23(1), 155-165 (2006).
[8] Goray, L. I., "Numerical analysis of the efficiency of multilayer-coated gratings using integral method," Nucl. Instrum. Meth. A 536(1-2), 211-221 (2005).
[9] Goray, L. I. and Sadov, S. Yu., "Numerical modeling of coated gratings in sensitive cases," OSA TOPS 75, 365-379 (2002).
[10] Goray, L. I., "Rigorous solution for electromagnetic scattering from multilayer structures having asperities of any kind in X-ray–EUV ranges," Proc. SPIE 6617, 661719-1-12 (2007).
[11] Goray, L. I., "A boundary integral equation method in short-wavelength-to-period diffraction on multilayer 1D gratings and rough mirrors," Proc. of the Int. Conf. Days on Diffraction, 60-65 (2008).
[12] Rathsfeld, A., Schmidt, G. and Kleemann, B. H., "On a Fast Integral Equation Method for Diffraction Gratings," Commun. Comput. Phys. 1, 984-1009 (2006).
[13] Kleemann, B. H. and Erxmeyer, J., "Independent electromagnetic optimization of the two coating thicknesses of a dielectric layer on the facets of an echelle grating in Littrow mount," J. Mod. Opt. 51(14), 2093-2110 (2004).
[14] Neviere, M. and Popov, E., [Light Propagation in Periodic Media: Differential Theory and Design], Marcel Dekker, New York (2002).
[15] Popov, E., Bozhkov, B., Maystre, D. and Hoose, J., "Integral method for echelles covered with lossless or absorbing thin dielectric layers," Appl. Opt. 38(1), 47-55 (1999).
[16] Kleemann, B. H., Gatzke, J., Jung, Ch. and Nelles, B., "Design and efficiency characterization of diffraction gratings for applications in synchrotron monochromators by electromagnetic methods and its comparison with measurement," Proc. SPIE 3150, 137-147 (1997).
[17] Saillard, M. and Maystre, D., "Scattering from metallic and dielectric surfaces," J. Opt. Soc. Am. A 7(6), 982-990 (1990).
[18] Maystre, D., Neviere, M. and Petit, R., [Electromagnetic Theory of Gratings], Petit, R., ed., Springer, Berlin, 159-225 (1980).
[19] Website, http://www.pcgrate.com
[20] Tsang, L., Kong, J. A., Ding, K.-H. and Ao, C. O., [Scattering of Electromagnetics Waves: Numerical Simulations], Wiley, New York (2001).
[21] Goray, L. I., Chkhalo, N. I. and Cirlin, G. E., "Determination of facet angles and heights of quantum dots from the analysis of diffuse and specular x-ray scattering," Technical Physics 79(4), 117-124 (2009).
[22] Stearns, D. G., Gaines, D. P., Sweeney, D. W. and Gullikson, E. M., "Nonspecular x-ray scattering in a multilayer coated imaging system," J. Appl. Phys. 84(2), 1003-1028 (1998).
[23] Boer, D. K. G., "Influence of the roughness profile on the specular reflectivity of x rays and neutrons," Phys. Rev. B 49(9), 5817-5820 (1994).
[24] Spiller, E., [Soft X-ray Optics], SPIE Press, Bellingham (1994).
[25] Saillard, M., Maystre, D. and Rossi, J. P., "Microrough surfaces: influence of the correlation function on the speckle pattern," Optica Acta 33(9), 1193-1206 (1986).
[26] Goray, L.I, "Application of the boundary integral equation method to very small wavelength-to-period diffraction problems," submitted to Waves Random Complex Media (2009).
[27] Li, L., "Formulation and comparison of two recursive matrix algorithms for modeling layered diffraction gratings," J. Opt. Soc. Am. A 13(5), 1024-1035 (1996).
[28] Maystre, D., "Electromagnetic study of photonic band gaps," Pure Apl. Opt. 3, 975-993 (1994).
[29] Schmidt, G., "Integral equations for conical diffraction by coated gratings," Preprint of WIAS No. 1296, 1-23 (2008).
[30] Goray, L. I. and Schmidt, G., "Integral-equation conical solver: some formulas and numerical experiments," Int. Conf. Days on Diffraction, May 26-29, St. Petersburg, Russia (2009).
[31] Born, M. and Wolf, E., [Principles of Optics], Pergamon, Oxford (1980).
[32] Website, http://www.cxro.lbl.gov/optical_constants/
[33] Goray, L. I., Chkhalo, N. I. and Vainer, Yu. A., "Grazing-incidence X-ray reflectometry for structural characterization of samples containing Ge/Si quantum dots," Proc. 17th Int. Symp. Nanostructures: Physics and Technology, Minsk, Belarus, June 22-27 (2009).